Mercaptolated Chitosan/Methacrylate Gelatin Composite Hydrogel for Potential Wound Healing Applications

Qiaoyun Wu[a,†], Ling Wang [a,†], Peng Ding[a,†], Yaling Deng[b], Oseweuba Valentine Okoro[c,*], Amin Shavandi[c,*], and Lei Nie[a,c,*]

[a] College of Life Sciences, Xinyang Normal University, Xinyang 464000, China

[b] College of Intelligent Science and Control Engineering, Jinling Institute of Technology, Nanjing 211169, P. R. China

[c] Université libre de Bruxelles (ULB), École polytechnique de Bruxelles, 3BIO-BioMatter, Avenue F.D. Roosevelt, 50 - CP 165/61, 1050 Brussels, Belgium

[†] These authors contributed equally to this work and should be considered co-first authors.

*** Corresponding author I: Prof. Lei Nie**

Post address: College of Life Sciences, Xinyang Normal University (XYNU), Xinyang 464000, China. Tel: +86-13600621068. ORCID: 0000-0002-6175-5883

E-mail address: nieleifu@yahoo.com; nielei@xynu.edu.cn

*** Corresponding author II: Dr. Oseweuba Valentine Okoro**

Post address: Université libre de Bruxelles (ULB), École polytechnique de Bruxelles, 3BIO-BioMatter, Avenue F.D. Roosevelt, 50 - CP 165/61, 1050 Brussels, Belgium

E-mail address: oseweubaokoro@gmail.com

*** Corresponding author III: Prof. Amin Shavandi**

Post address: Université libre de Bruxelles (ULB), École polytechnique de Bruxelles, 3BIO-BioMatter, Avenue F.D. Roosevelt, 50 - CP 165/61, 1050 Brussels, Belgium

E-mail address: amin.shavandi@ulb.be

Abstract

In this study, medical hydrogels (TGs) were fabricated based on thiolate-modified chitosan (TCS) and methacrylate gelatin (GelMA) using the Thiol-Michael addition reaction. The hydrogels were formed via the Michael reaction between TCS and GelMA and determined to have an equilibrium swelling rate of more than 1100 % while simultaneously providing a moist environment for the wound, and limiting crust formation. The porosity of the prepared hydrogel was also shown to have a positive correlation with the concentration of the thiolated chitosan in the formulation. A positive correlation between hydrogel strain and stress properties and increasing concentrations of thiolated chitosan was also observed. The cytocompatibility of the prepared hydrogels was also tested and confirmed using CCK-8 assay after 5 days of culture, and the best antimicrobial properties were observed with the hydrogel containing TCS and GelMA in the mass ratio of 1:2. The present study was, therefore, able to highlight the potential of a simple and low-cost approach to developing cytocompatible hydrogels with antibacterial properties and tunable mechanical properties based on the well-studied GelMA. This study implies that the produced hydrogels can have future applications in fabricating skin wound healing dressings.

Keywords

Hydrogels; chitosan; GelMA; cytocompatibility; antibacterial properties.

1 Introduction

Chitin, as the second most abundant biopolymer after cellulose, has been widely studied for diverse applications in different sectors such as including food, environment, and biomedical sectors [1, 2]. In biomaterials engineering, its derivative chitosan has been fabricated into injectable hydrogels, sponges and scaffolds, microbeads, and hydrogels [3]. Chitosan-based hydrogels have gained much interest for cell encapsulation, drug delivery and soft tissue engineering due to their favourable biological and physicochemical properties such as cell compatibility, antimicrobial properties, biodegradability in physiological solutions, and favourable cell attachment properties [4]. The functional chitosan-based hydrogels could be accomplished by chemical modification or compositing with other components. Chitosan could be chemically modified using its inherent reactive activity due to the presence of hydroxy- or amino functional groups. Major reactions in this regard are acylation, carboxymethylation, quaternization, sulfation, N-phosphomethylation etc [5-9]. Indeed, chitosan has also been cross-linked with glutaraldehyde or glycerophosphate or composited with other polymers, including alginate and gelatin [10, 11]. Notably, it was previously reported that modified chitosan such as *N*-succinyl, aldehyde, hydroxyethyl, hydroxypropyl and phenolated chitosan hydrogels could be employed for drug delivery [12], bone tissue engineering [13-15], cell encapsulation [16] and wound healing applications [17-19].

The rapid and selective reaction under physiological conditions is important for the formation of hydrogels in biomedical applications, such as wound healing dressings [19]. The efficient “click” chemistry, such as Michael addition reaction, holds a great potential to address the above challenges [20, 21]. Teng *et al.,* [22] fabricated in situ cross-linked hydrogels based

on thiol-modified chitosan and PEG diacrylate (PEGDA) via Michael type addition. The gelation time and elasticity of the prepared hydrogel depended on the content of thiol-modified chitosan. It was also acknowledged that gelatin methacrylate (GelMA) constitutes the most widely investigated photo cross-linkable biopolymer for hydrogel fabrication due to its favourable mechanical properties, gelation, cell cytocompatibility and cell attachment properties [23, 24]. The present study sought to integrate the beneficial properties of GelMA with thiolate-modified chitosan to produce a novel hydrogel. In the study, a biologically active hydrogel system with multi crosslinking abilities comprising of thiolate-modified chitosan (TCS) and gelatin methacrylate (GelMA) based on methacrylate-thiol (click) chemistry, was developed, shown in **Scheme 1**. Since monomers with activated double bonds such vinyl sulfones, vinyl esters, maleimides and imidazoles can undergo Michael addition with nucleophiles such as thiol or amine. The present study proposes that the Michael addition reaction between thiol of the modified chitosan and methacrylate of GelMA will facilitate the synthesis of the hydrogel under mild conditions since GelMA undergoes radical polymerization in the presence of light and a photoinitiator. It is anticipated that the hydrogel generated could have the potential as a wound dressing if its cell cytocompatibility and mechanical properties are determined to be sufficient.

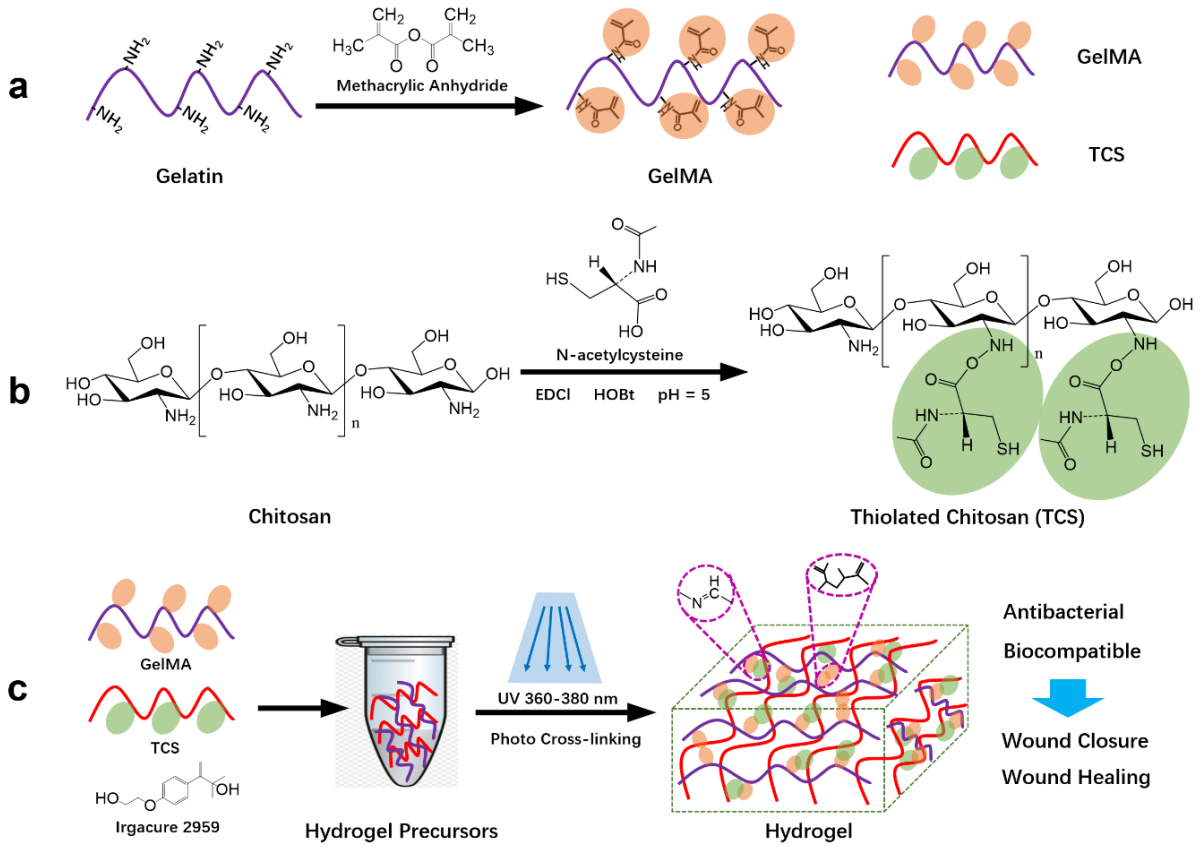

Scheme 1. Schematic of thiolated chitosan/methacrylate gelatin (TG) hydrogel. (**a**) Synthesis of gelatin methacrylate (GelMA); (**b**) Preparation of thiolated chitosan (TCS); (**c**) The preparation principle of composite TG hydrogel, under the condition of ultraviolet light irradiation.

2 Material and methods

2.1 Material

Chitosan (CS, SKU: 448877) with 80-95% deacetylation degree and 50-800 cP viscosity was purchased from Sigma-Aldrich Chemical Reagent Co., Ltd. Gelatin (Gel, Catalog Number: 10010326), sodium chloride (NaCl), sodium hydroxide (NaOH), and hydrochloric acid (HCl) were purchased from Sinopharm Chemical Reagents Co., Ltd. 1-hydroxybenzotriazole

($C_6H_5N_3O$, HOBt) and 1-ethyl-3-(3-dimethyl-amino-propyl-carbon diimine) hydrochloride ($C_8H_{18}ClN_3$) were purchased from RON reagent Co., Ltd. N-acetylcysteine (NAC) was purchased from McLean Biochemical Co., Ltd. Ethylenediamine tetraacetic acid ($C_{10}H_{16}N_2O_8$) was purchased from Tianjin Bodi Chemical Co., Ltd. Durbeco phosphate buffer salt (D-PBS) and methacrylic anhydride ($C_8H_{10}O_3$, EDCl) were purchased from Aladdin Co., Ltd. Irgacure2959 was purchased from Guangyi Chemical Co., Ltd. Fetal bovine serum, Trypsin, Penicillin, Streptomycin mouse fibroblasts, *Escherichia coli* and *Staphylococcus aureus* were all obtained from Wuhan Huashun Biotechnology Co., Ltd. All reagents were purchased and used directly without further purification.

2.2 Methods

2.2.1 Thiolated chitosan (TCS) preparation

TCS was synthesized according to the previous literature with further modification [25]. 1 g CS was dispersed in deionized water (92 mL) after which 1-hydroxybenzotriazole (HOBt) (0.6972 g, 2.58 mM) was added. The mixture was then stirred until a clear solution was observed. N-acetyl cysteine (NAC) (1.684 g, 5.16 mM) and EDCl solution (3.957 g, 10.32 mM, 8mL) were subsequently added to the mixture, and the pH of the reaction mixture was adjusted to 5 via the dropwise introduction of 1M HCl. The mixture was then stirred on a magnetic stirring platform (DF-101S, Zhengzhou), and incubated at room temperature for 3 h. The incubated solution was dialyzed （dialysis bag 7000 Da） in the dark at 4 ºC for 3 d, using different solutions. Specifically, on the first day, 5 mM HCl and 2 μM EDTA were used as dialysate. On the second day, a mixture of 5 mM HCl, 2 μM EDTA and 1% NaCl was used as dialysate. On the third day, 1 mM HCl solution was used as dialysate. After dialysis, the samples

were freeze-dried in a freeze-dryer (FD-1C-50, Shanghai) and then stored at 4 ºC.

2.2.2 Methacrylate gelatin (GelMA) preparation

GelMA was synthesized according to the previous literature [26]. A 10% (w/v) gelatin solution was initially prepared by mixing 5 g gelatin and 45 g D-PBS at 50 ºC until it was completely dissolved and adjusting the solution pH to neutral via the dropwise addition of 0.1 M NaOH. Then a 20 v/v % of 5 mL methacrylate anhydride was prepared with D-PBS, and slowly added into a gelatin solution at 50 ºC. During this process, the pH of 7 was maintained with continuous stirring (600 r/min) imposed for 2 h. Finally, 5-fold diluted D-PBS was added to stop the reaction, and the mixture was dialyzed in deionized water at 40 ºC for one week in a 12-14 kDa dialysis bag. The solution was freeze-dried for 1 week, and the dried product was stored at -80 ºC.

2.2.3 TCS/GelMA (TG) hydrogel fabrication

The composite TG hydrogels were prepared by combining TCS with GelMA (**Scheme 1**). TCS and GelMA were dissolved in deionized water. After then, irgacure 2959 (photoinitiator, 5% of the mass of GelMA) was then added under dark conditions and thoroughly mixed. The mixed solution was exposed under UV-light irradiation (45 mW/cm^2) to obtain TG hydrogel. The prepared hydrogels were designated TG01, TG11, TG12, and TG21, while the mass ratios of TCS and GelMA were 0:1, 1:1, 1:2 and 2:1. The polymer concentration for preparing TG01 hydrogel was 5 wt%, and the gelatin time was 120 s. The polymer concentrations of other TG11, TG12, and TG21 hydrogel were 2.5 wt%, and the gelation times were around 90 s.

2.2.4 Attenuated total reflectance-Fourier transform infrared spectroscopy (ATR-FTIR) analysis

Attenuated total reflectance-Fourier transform infrared spectroscopy (ATR-FTIR, ThermoFisher, Nicolelis5) was used to analyze the presence of specific chemical groups in prepared TG hydrogels. The CS, TCS, gelatin and GelMA were also analyzed and compared. The FTIR spectra were obtained within the range between 500 and 4000 cm^{-1} with a resolution of 1 cm^{-1}, with each spectrum averaged over 64 scans, using the ATR technique.

2.2.5 Nuclear magnetic resonance (NMR) analysis

The samples were dissolved in D_2O, respectively, and the dissolved samples were transferred into the nuclear magnetic tube. The optimal height of the sample in the NMR tube was 4 cm. H-spectrum then tested the prepared samples on the Nuclear magnetic resonance spectrometer (^{1}H NMR 600 MHz NMR spectrometer, JEOL ECZ600R/S3) to calculate the degree of thiol substitution of TCS and the degree of double bond substitution of GelMA.

2.2.6 Scanning electron microscopy (SEM) analysis

The freeze-dried hydrogel samples were cut into thin slices of uniform thickness and size, and adhered on the sample table using a conductive glue. The edge of the sample was gently pressed using the tip of tweezers to prevent the sample from falling off and then spray coated with a thin platinum conductive layer on its surface. The microstructure of TG hydrogels was observed under Cold Field Scanning Electron Microscopy (SEM, S-4800, Hitachi).

2.2.7 Porosity analysis

The porosity, *P*, of each TG scaffold was calculated using the liquid displacement method [27]. The dried TG scaffold was immersed in a known volume (V_1 in mL) of ethanol. The total

volume of support and solution was denoted as V_2 in mL. After 20 min, the scaffold was removed, and the remaining ethanol volume, V_3 in mL, was measured. The porosity was then calculated as follows:

$$P = \frac{V_1 - V_2}{V_2 - V_3} \times 100\% \quad (1)$$

2.2.8 Swelling properties analysis

The equilibrium swelling ratio of each TG hydrogel was measured in PBS (pH = 7.4) at room temperature. The dried hydrogel, with a mass of W_1 in g, was soaked in PBS solution and weighed every 10 min. The excess liquid on the sample was removed using an absorbent paper, and the mass of the sample, W_2 in g, was recorded until a constant mass was attained. The equilibrium swelling ratio was then calculated as follows [28];

$$S = \frac{W_2 - W_1}{W_1} \times 100\% \quad (2)$$

Before the hydrogels reached to equilibrium swelling ratio, the samples were retrieved at a pre-designated time, and the swelling ratio was calculated to obtain the swelling kinetics of TG hydrogels [29].

2.2.9 Rheological test

The rheological properties of the TG hydrogels were tested using a DHR-2 rheometer (TA, USA). Frequency, shear, self-healing and stress tests were carried out using a 40 mm diameter and 1 mm clearance aluminium low inertia parallel plate. In order to avoid evaporation of water from the sample during the test, the edge of the fixture was sealed using glycerin. To determine the linear viscoelastic region of TG hydrogel, the energy storage modulus (G') and loss modulus (G") of TG hydrogels were measured by varying the strain in the range of 0.1 ~ 600 % at a

frequency of 1 Hz. After the linear viscoelastic zone was determined, the G' (store modulus) and G" (loss modulus) of TG hydrogels were measured at room temperature in the range of 0.1 ~ 100 rad/s angular frequency. Linear frequency scanning was carried out in the strain of the selected linear zone in the range of 0.1 ~ 200 rad/s. Steady-state shear rates ranging from 10^{-3} to 10^{3} s^{-1} were imposed to determine the relationship between TG viscosity, stress, and shear rate.

2.2.10 Antibacterial test

E. coli and *S. aureus* are the most common gram-negative and positive bacteria in clinical wound infection, respectively. Therefore, this study used *E. coli* and *S. aureus* to test the antibacterial performance of the TG hydrogel as wound dressing material. The two strains were cultured in LB broth medium for 24 h and diluted to 2×10^{8} CFUs/ mL. TG hydrogels were cut into 6 mm in diameter and 2 mm in height, and placed on an NA medium filled with 100 μL bacterial solution. The culture mixture was then incubated at 37 ºC for 12 h, and the size of the inhibition zone was observed.

At the same time, the freeze-dried hydrogel sample was weighed (0.002 g) and put into the glass tube, and 10 mL of the above diluted bacterial solution was added. The antibacterial tests were repeated thrice for each sample, and the bacterial solution without the sample was employed as the control group. The culture mixture was then incubated at 37 ºC for 12 h. The color of the culture medium was observed, and the optical density (O.D) value at 600 nm was measured.

2.2.11 NIH-3T3 cells culture

NIH-3T3 cells (CRL-1658™, ATCC) were cultured in this experiment. According to

ATCC instructions, the frozen NIH-3T3 cells were first resuscitated. The frozen tubes were removed from liquid nitrogen and immersed in water at 40 ºC for rapid thawing, and the frozen tubes were then removed after complete thawing. After cleaning the entrance of the tube with 75 v/v% alcohol, the cryoprecipitate tube was opened, and the supernatant was collected. This supernatant was then centrifuged to enable the collection of cells. The cells were washed once in a serum-free medium and cultured in Dulbecco modified Eagle's medium that was supplemented with 10 % fetal bovine serum and 1 % penicillomycin mixture in a CO_2 incubator at 37 ºC, with daily cell growth recorded. The medium was changed every 2 d, and the cells were subcultured by the trypsinization method. The 5^{th}-generation cells were then recovered and used for the cell viability test.

2.2.12 CCK-8 assay

The CCK-8 assay was used to evaluate the cytocompatibility of TG hydrogels by culturing them with NIH-3T3 cells. The cell viability of cultured scaffolds was quantitatively studied by measuring the O.D of cultured scaffolds. Each scaffold was cut into a circular disk with a diameter of 8 mm, kept in 75 v/v% ethanol for sterilization, and then washed with sterile PBS. The NIH-3T3 cells (1×10^4 cells /mL) were inoculated on a 48-well plate (Corning).

According to the instructions of the CCK-8 kit, 10 μL CCK-8 kit solution was initially added to the sample, and rigorously agitated. The mixture was then incubated in a CO_2 atmosphere for 4 h. The reacted orifice plate was retrieved, and the liquid in the orifice plate moved to a new orifice plate. Cells cultured directly in a culture medium without adding hydrogels were used as a blank control group. The O.D value of each orifice in the new orifice plate at 450 nm was measured using a microplate reader (SpectraMax 190, USA). Prior to

CCK-8 staining, cell growth on the scaffold was observed with an inverted microscope (TI2-E, Nikon).

2.2.13 Cell fluorescence test

The orifice plate cultured on days 1, 3, and 5 was retrieved, the culture liquid in the orifice plate was collected, and PBS was employed in cleaning the orifice plate. First, 2.5 % glutaraldehyde was added to localize the cells on the scaffold. After the localization, the cells were rinsed twice with PBS to remove the excess glutaraldehyde. Secondly, 0.2 v/v% Triton-100 solution was added to hydrogels, and the mixture was stored for 10 min. The Triton-100 was then desorbed, and washed, using PBS, twice. 5 μL of photoleptide stock solution was diluted to 2.5 % using PBS, and the obtained solution was added to the well plate with 1 % bovine serum albumin solution and stored at room temperature for 1 h. The liquid was then removed, and the residue was washed twice with PBS. Finally, phalloidin-FITC and 4'6-diamidino-2-phenylindole (DAPI, Thermo Scientific^{TM}) were used according to the supplier's instruction and then cleaned with PBS twice. The hydrogels were observed under a confocal laser microscope (CLSM, Leica TCS SP5 II, Germany) at wavelengths ranging from 360 nm-400 nm.

2.2.14 Statistical analysis

Each experiment is repeated three times. Values were presented as the means of these replicates ± standard error of the mean. Mean values were compared by one-way analysis of variance (ANOVA) using SPSS.22 statistical software package, LSD method was used for pairwise comparison with statistical significance established when $p < 0.05$.

3 Results and discussion

3.1 TG hydrogel physicochemical characterization

The ^{1}H NMR spectra of gelatin and GelMA are shown in **Figure 1a**. The GelMA spectra showed two new peaks, designated as 'a' and 'b' at 5.4 ppm and 5.6 ppm, respectively, compared to the gelatin spectra. This observation is due to the double bond structure of the methacrylic acid [30]. The area integral of the two new peaks was determined to be 0.07 and denoted as A3. The peak designated as c at 0.8ppm represents the characteristic peak of gelatin, due to the presence of amide groups, with the integrated peak area calculated to be 0.42 and designated as A4. The amino substitution degree of methacrylic anhydride on the side chain of gelatin, was calculated as the percentage of A3 relative to A4 and determined to be 16.7 %. The ^{1}H NMR spectra of TCS and CS are also shown in **Figure 1b**. **Figure 1b** shows that the characteristic peak of the position designated as 1 is at 3.18 ppm, and the integrated area, A1, relative to the total area, is determined to be 24.26 %. The characteristic peak at position 2, was detected at 2.93 ppm, which was the methylene protons connected with the thiol group, indicating that cysteine was successfully grafted to the chitosan sugar ring, and the thiol group had been successfully introduced. The integrated area of the peak at position 2, A2, relative to the total area, was determined to be 1.00 %. The methyl peak at three sites (2.0-2.1 ppm) was significantly enhanced, indicating that NAC had been coupled with chitosan [31]. The mercapto substitution degree, was obtained as the percentage of A2 relative to A1 and determined to be 4.1%.

Figure 1c shows the spectra of gelatin and Gel-MA. The spectrum of gelatin shows a peak at 3443 cm^{-1} due to N-H stretching of secondary amide and N-H swinging out of the plane

at 665 cm^{-1} [32]. Pure gelatin shows a series of amide (1240 cm^{-1}, 1543 cm^{-1} and 1650 cm^{-1}) and carboxyl (1300-1450 cm^{-1}) bands, which are attributed to amino acids in the main chain of gelatin, such as glycine, proline and hydroxyproline. The peaks of GelMA appeared between 1600-1700 cm^{-1}, which could confirm the existence of double bonds in the modified gelatin. The results show that the double bond modification of gelatin is successful.

As shown in **Figure 1d**, chitosan peaks detected at 3359 cm^{-1}, 3475 $cm^{-1,}$ and 3409 cm^{-1} arise due to vibrations of primary amine (-NH_2) and hydroxyl (-OH) groups [32]. For TCS, these peaks transform into a new single peak of 3443 cm^{-1}, caused by tensile vibration of -OH and secondary amine (-NH) on thiolated functionalized chitosan [32]. In addition, the S-S tensile peak in the frequency range of 560-570 cm^{-1} confirmed the presence of disulfide bonds in the ligands on the chitosan framework. The spectra also show peaks at 1630 cm^{-1} and 1530 $cm^{-1,}$ indicating the presence of C=O and N-H bending frequencies[32]. These peaks also show increased amide bonds on the modified polymer. According to these results, the covalent binding of the two ligands can be qualitatively determined, indicating that the thiolation modification of chitosan was successful.

According to the results of ^{1}H NMR and FTIR, it was determined that TCS and Gel-MA were successfully prepared. **Figure 1e** shows the photos of TG01, TG11, TG12, and TG21 hydrogels, and the formation of TG hydrogel could be evaluated by a tube inversion method [33, 34]. The formation of TG hydrogel is attributed to the cross-linking of TCS, GelMA itself and the chemical click reaction between TCS and GelMA. The Michael addition interaction between thiol groups of the modified chitosan and methacrylate groups from GelMA results in cross-linking and hydrogel formation (**Scheme 1** and **Figure 1f**). The peak at 1720 cm^{-1} was

attributed to the carbonyl stretching vibrations of methacrylate moiety, due to that, the thiol addition on the double bond could reduce its conjugation to the adjacent carbonyl group [20, 35]. The covalent bonding between Gel-MA and TCS provides the required binding property for hydrogels.

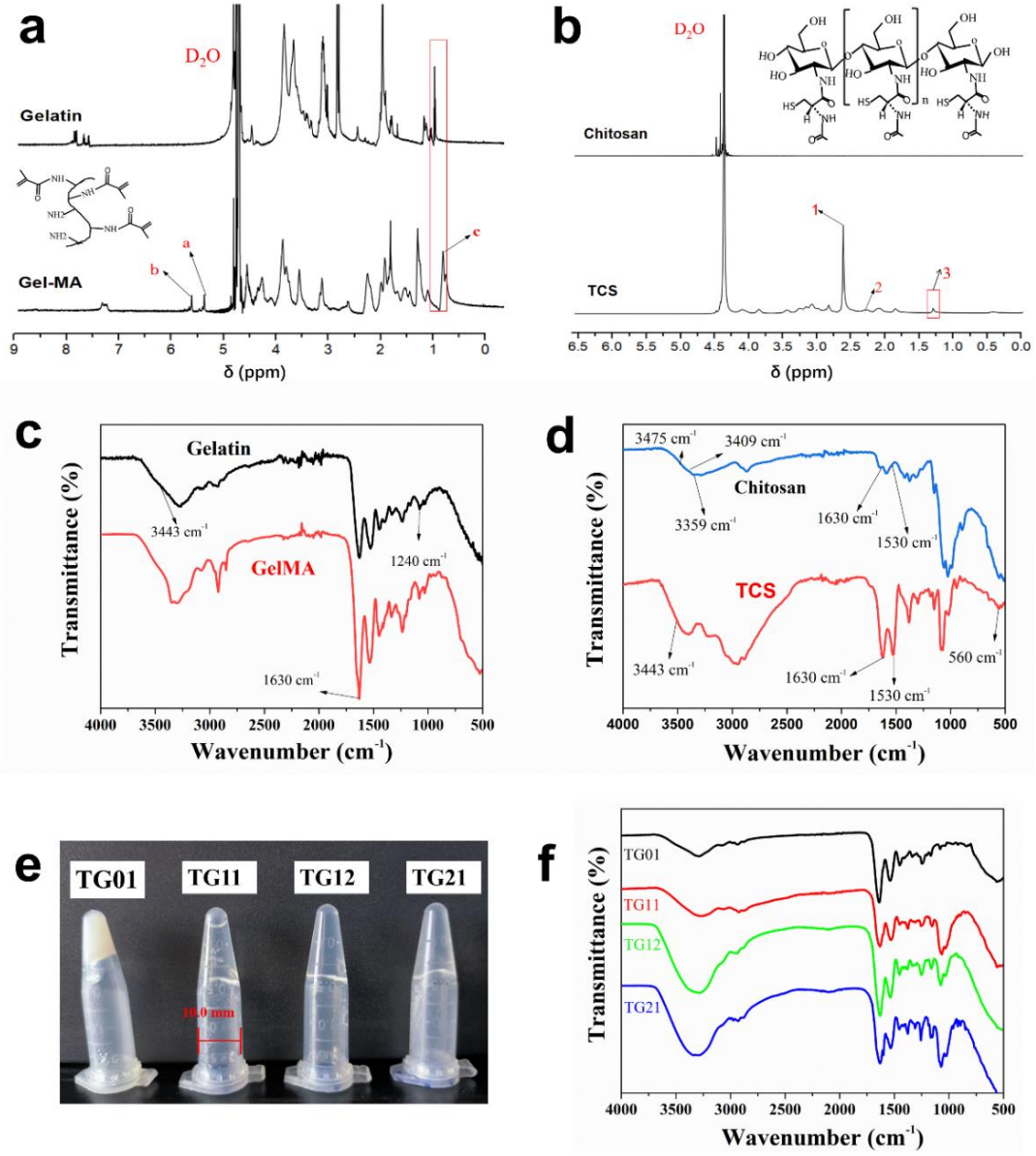

Figure 1. (**a**) ^{1}H NMR spectra (D_2O) of gelatin and GelMA. (**b**) ^{1}H NMR spectra (D_2O) of chitosan and TCS. (**c**) FT-IR spectra of gelatin and GelMA. (**d**) FT-IR spectra of chitosan and TCS. (**e**) Macroscopic images of the formed TG hydrogels compositing TCS and GelMA solutions, the hydrogel formation was identified using the tube inversion method. (**f**) FT-IR spectra of TG hydrogels, TG01, TG11, TG12, and TG21.

3.2 Morphology of TG hydrogels

The cross-sectional morphologies of the TG hydrogels were observed by SEM, as shown in **Figure 2a-h**. The hydrogels were determined to have a connected structure, which supports the growth of granulation in the wound and can inhibit the growth of anaerobic bacteria. It can also be seen that various components are evenly distributed on the surface of the gel, without clustering or stacking, indicating that TCS and GelMA in the hydrogels participate in the reaction and evenly form the gel. The cross-linking density greatly influenced the morphology of hydrogels, and the pore size was usually decreased with the increase of cross-linking density [36, 37]. The formation of TG hydrogels was attributed to the cross-linking of GelMA, and the cross-linking between TCS and GelMA. Sample TG12 hydrogel used the mass ratio of TCS/GelMA at 1:2 and displayed a different porous morphology compared to other samples, mainly due to the different cross-linking sites and cross-linking density.

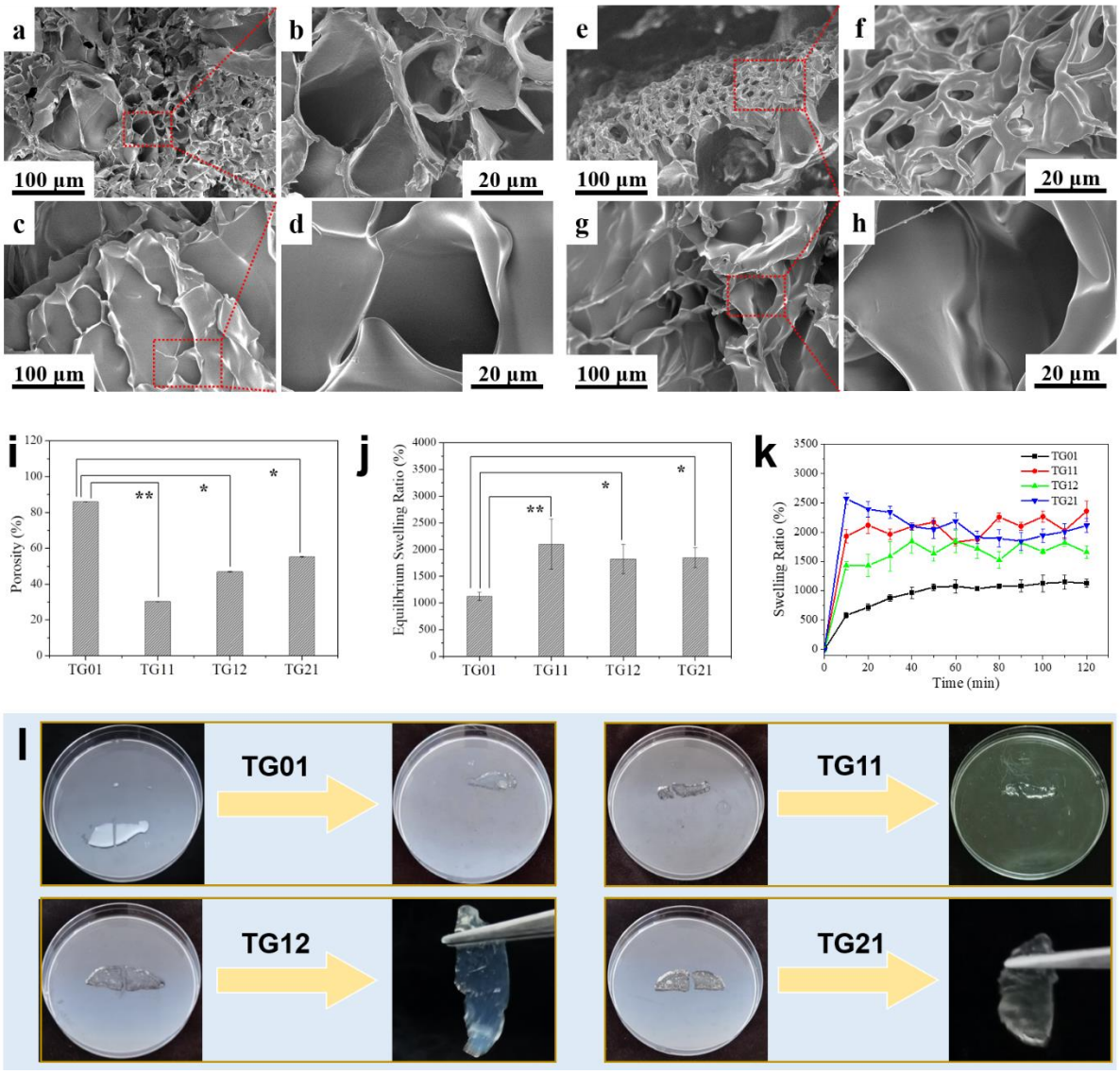

Figure 2. Scanning electron microscope images of TG hydrogels, the cross-sectional morphology was observed for all samples, (**a, b**) TG01; (**c, d**) TG11; (**e, f**) TG12; and (**g, h**) TG21. (**i**) Porosities, (**j**) equilibrium swelling ratios, and (**k**) swelling kinetics of the TG hydrogels. *p < 0.05 and **p < 0.01. (**l**) TG hydrogels were cut into two pieces, and the hydrogels can self-healed after contact for 30 min without external intervention.

3.3 Porosity, swelling and self-healing properties

Figure 2i shows that the porosity of all composite TG hydrogels is greater than 30 % and ranges from 30.3 % to 85.9 % for TG01 and TG11, respectively. **Figure 2i** also highlights the

dependence of the porosity of hydrogel on variations in the concentrations of TCS. **Figure 2j** also shows that the equilibrium swelling ratios of all TG hydrogels in PBS are above 1100 %, with the TG11 and TG01 hydrogels having the highest and lowest equilibrium swelling ratios of 2100.2 % and 1124.3 %, respectively. In addition, the swelling kinetics of TG hydrogels were displayed in Figure 2k; the swelling ratios of all TG hydrogels were quickly increased in the first 10 min, and then arrived to an equilibrium swelling ratio in 30 min. TG11, TG12 and TG21 hydrogels displayed a quicker solution absorbing ability than TG01 hydrogel, due to that, the hydrophilicity of hydrogel was increased in addition of TCS. The above results show that all TG hydrogels can quickly absorb a large amount of blood and wound exudate, indicating their capacity to keep the wound clean, and can provide a moist environment for the wound, thus avoiding dehydration. The equilibrium swelling ratios of TG hydrogels were related to TCS/GelMA ratio since the equilibrium swelling rate of pure methacrylate gelatin hydrogel was improved by adding TCS (50 wt.%). Indeed, for the scenario of the TG hydrogel containing 50 wt.% of TCS, the hydrogel TG11, presented the highest equilibrium swelling rate of 2100 %.

Further increments in the TCS content in TG12 and TG21, did not however translate to significant changes in equilibrium swelling rate. Furthermore, the self-healing performance of TG hydrogel was displayed (**Figure 2l**). After being destroyed or divided, the self-healing hydrogel could be recovered in a short time. In this work, the TG hydrogel was cut and divided into two parts, after the divided parts were contacted for 30 min, the TG hydrogels could be self-healed, maintaining the integrity of the hydrogel. Especially for samples TG12 and TG21, the hydrogels could be suspended using a forcep.

3.4 Rheological properties analysis

The rheological properties of the hydrogel are shown in **Figure 3**. **Figure 3** shows that as the shear frequency imposed increases, negligible changes in the storage modulus of TG01 are observed as the loss modulus increases. However, for the TG11, TG12, and TG21 hydrogels, an increase in shear frequency translates to an increase in the storage and dissipation moduli, with the hydrogels of TG11 and TG12 presenting the most significant loss modulus and storage modulus, respectively.

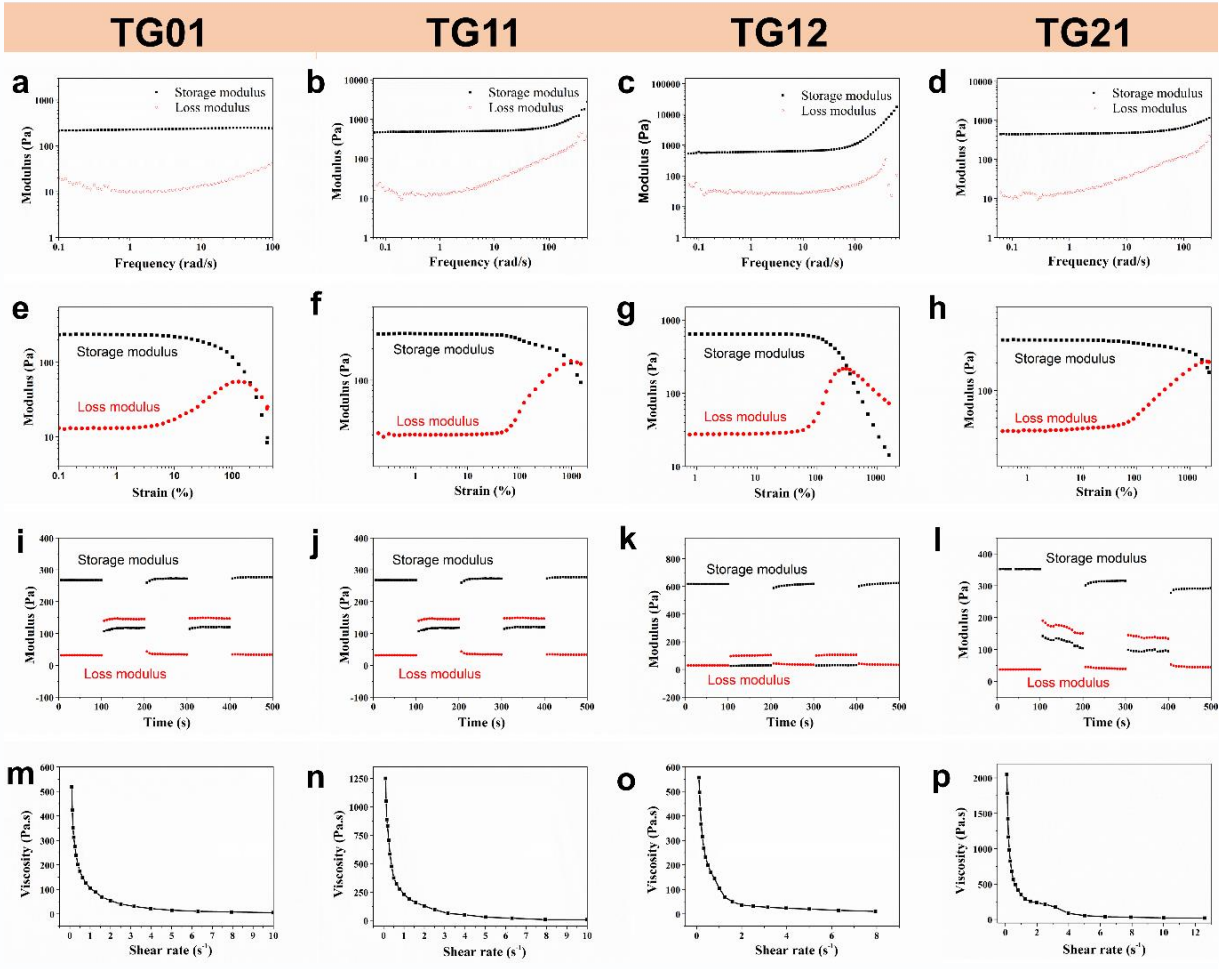

Figure 3. Rheological properties of the prepared TG hydrogels. The storage modulus (G') and loss modulus (G'') were evaluated over (**a**, **b**, **c**, and **d**) frequency, (**e**, **f**, **g**, and **h**) strain, and (**i**, **j**, **k**, and **l**) time. (**m**, **n**, **o**, and **p**) The change of viscosity of TG hydrogels in terms of shear rate.

All hydrogels displayed the expected hydrogel behaviour with the G' (storage modulus) shown to be greater than G" (loss modulus), when stress is initially imposed. A sustained increase in stress, however, was observed to lead to the G' and G" coinciding, followed by a subsequent overlap, indicating a breakdown in structure. While G' shows greater than G", indicating the hydrogels' solid state and elastic deformation [16]. **Figure 3** also shows that magnitude of the strain that can be tolerated by the hydrogels before 'structural failure' increases as follows; TG01 > TG11 > TG12 > TG21. This trend also implies that the stress and strain capacity of the hydrogel increases as the concentration of mercapto chitosan (from TCS and GelMA) increases. In terms of the hydrogel self-healing performance of hydrogels, after 100 s recovery time, the hydrogels showed a good self-healing performance. The storage moduli of TG01, TG11 and TG12 were also shown to be retained healing, indicating that the hydrogels maintained their internal structure. Further application of stress may lead to a reduction in the storage modulus and self-healing ability over time due to intermolecular damage, as shown by TG21. The self-healing behaviour of TG hydrogels could also be observed while cut into two parts and re-contacted in 30 min (**Fiure 2l**). **Figure 3m-p** also shows that the apparent viscosities of the different TG composite hydrogels decreased as the shear rate increased, implying shear thinning behaviour. Interestingly, the decrease in the viscosity of the hydrogels was most profound in the TG 01 hydrogel, indicating that the electrostatic force existing between TCS and GelMA is the weakest. This observation also implies that the mechanical properties of pure methacrylate gelatin hydrogel were enhanced when TCS was introduced.

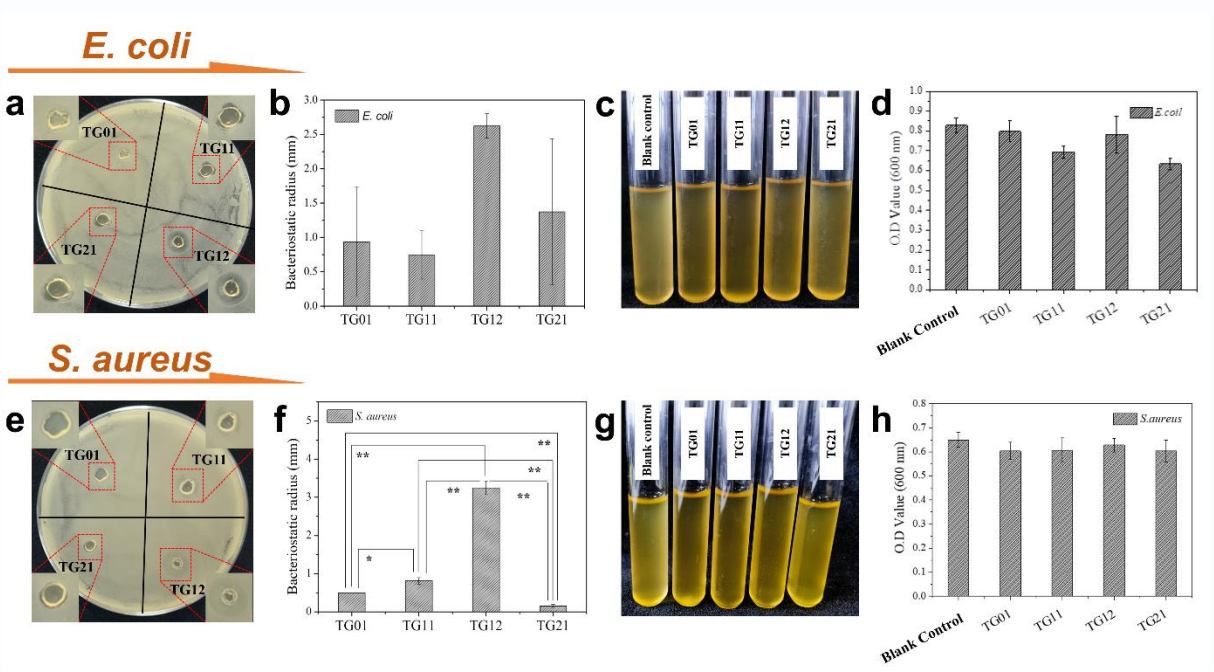

Figure 4. The antibacterial properties of the TG hydrogels. Antibacterial activities of TG hydrogels were confirmed using *E. coli* (**a**) and *S. aureus* (**e**) grown on nutrient agar plates, the images inserted on the corners for photos (**a**, **e**) were enlarged at a higher magnification, and the bacteriostatic radius for *E. coli* (**b**) and *S. aureus* (**f**) were measured. In addition, photos of *E. coli* (**c**) and *S. aureus* (**g**) grown in the actual culture tubes after the addition of TG hydrogels after 12 h, the optical density (OD_{600nm}) (**d**, **h**) were measured.

3.5 Antibacterial properties analysis

Antibacterial performance is an important prerequisite for hydrogel as skin dressing. The antibacterial results of TG hydrogels are shown in **Figure 4**. **Figure 4a** and **4e** show that bacteriostatic circles are present around the TG hydrogels after only 12 h, indicating the presence of an inhibitory effect on the growth of *E. coli* and *S. aureus*. For *E. coli*, the radius of the inhibition zone ranged from 0.75 mm to 2.63 mm, for TG11 and TG12, respectively (**Figure 4b**). Similarly, for *S. aureus*, bacteriostatic circles with a radius of the inhibition zones ranging from 0.16 to 3.25 mm were observed for TG21 and TG12, respectively (**Figure 4f**).

The result, therefore, shows that the hydrogel of TG12 has the strongest antibacterial effect against *E. coli* and *S. aureus.*

The O.D values of transmittance of *E. coli* and *S. aureus* at 600 nm after incubation for 12 h (**Figure 4c-h**) were further detected to confirm the antibacterial effects of the TG hydrogels since the O.D value presents converse relationships to the antibacterial performances. Compared with the blank control group without samples, the O.D value at 600 nm was lower in the culture medium containing the TG hydrogel samples. The antibacterial property of TG hydrogels was due to the contribution of cationic in TCS, which could interact with the negatively charged cell membrane and change the cell structure to cause the death of bacteria [38, 39]. With the increasing mass ratio of TCS and GelMA, the antibacterial property of TG hydrogels was increased first due to mercaptolated groups. However, with the continuous increase of the mass ratio of TCS and GelMA, more mercaptolated groups were cross-linked with GelMA, causing the decrease of antibacterial property for TG hydrogels. It is observed that TG12 produced the lowest O.D. value at 600 nm showing that it had the strongest antibacterial effect. The favourable antibacterial properties of the TG hydrogels suggest their potential for use in the fabrication of wound dressings.

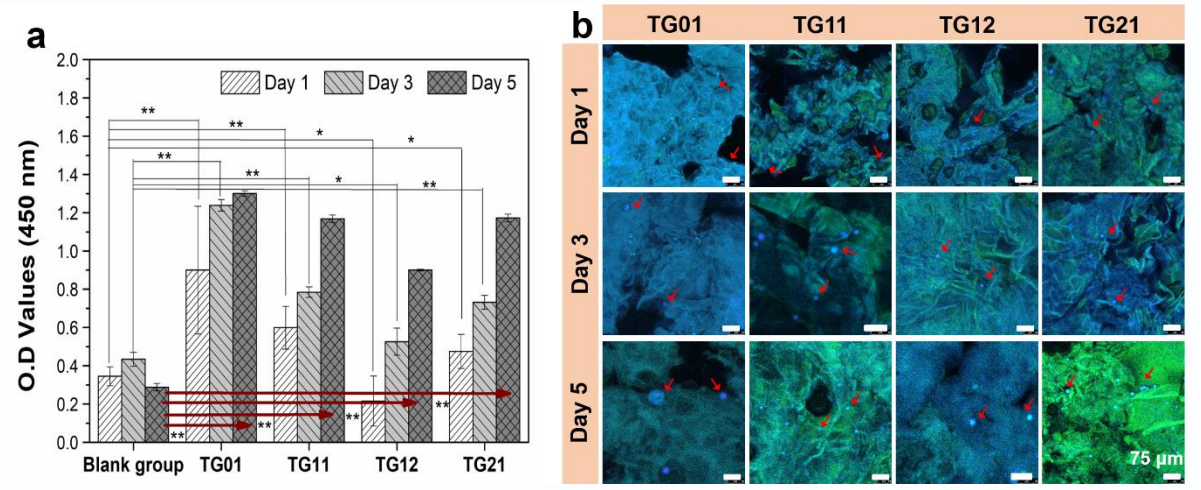

Figure 5. (**a**) Cytocompatibility of the prepared TG hydrogels was evaluated by CCK-8 assay by culturing with NIH 3T3 cells for different days with the control group. *p < 0.05, and **p < 0.01. (**b**) Representative fluorescent microscopy images of TG hydrogels cultured with NIH 3T3 cells for 1, 3, and 5 days, the samples were stained using phalloidin-FITC/DAPI. Red arrows indicate the observed NIH 3TC cells.

3.6 CCK-8 and fluorescent images analysis

The cytocompatibility of the TG hydrogels was studied using CCK-8 and fluorescent images. NIH-3T3 cells were seeded on the prepared hydrogels, cultured for 1, 3 and 5 days, and then treated with CCK-8 solution. ELISA detected the O.D value at 450 nm, and the presence of metabolically active cells was detected, as shown in **Figure 5a**. The growths of cells cultured on TG hydrogels on days 1, 3 and 5 were observed using a fluorescent microscope, as shown in **Figure 5b**. **Figure 5b** shows the differences in the cells in the culture medium, and the cells that adhere to the surfaces of the TG hydrogels via fluorescence detection of cells stained with DAPI dye solution. The adherence of the cells on the TG surface is due to the large size of NIH-3T3 cells. According to CCK-8 results (**Figure 5a**), the O.D values of all TG hydrogels increased over days, and compared to the control group, TG hydrogels displayed a higher O.D

value except for sample TG12 at day 1. Although cell growth varied with the composition of the TG hydrogel, in all cases, the cells were shown to be capable of proliferating on TG hydrogels. Our results are, therefore, in agreement with a previous study on thiolated chitosan-oxidized dextran hydrogel, which showed biocompatibility and non-cytotoxic behaviour of the double network hydrogel [40]. Notably, the capacity of the TG hydrogels to support NIH-3T3 cell proliferation, which is necessary for lesion repair and limiting the potential of hypertrophic scar and keloid formation, further supports the potential application of the TG hydrogels in wound healing applications.

4 Conclusion

In the present study, methacrylate gelatin (GelMA) and thiolated chitosan (TCS) were used to prepare hydrogels via the chemical click method. These hydrogels were subsequently assessed to measure their physicochemical, cytocompatibility and biological properties. The mass ratio of TCS and GelMA in the composite hydrogel influences porosity, equilibrium expansion rate and mechanical properties of TG scaffolds. The rheological tests also showed that the TG hydrogels had good mechanical and self-healing properties. The favourable antibacterial performance and cytocompatibility properties of the TG hydrogels were also established. Data from the above systems indicated that TG composite hydrogels have the potential to be applied as wound dressings in skin tissue engineering. The current study acknowledges the need for further investigations to establish the functionality of the TG hydrogel use in wound healing applications, to this regard, future studies will assess the wound healing rates of TG hydrogels using wounds in rat models. Comparative assessment of the TG

wound healing times and the natural healing wounds without treatment as control, will be undertaken.

Conflicts of Competing Interest

The authors declare no competing financial interest.

Acknowledgements

Lei Nie acknowledges the support from the Nanhu Scholars Program for Young Scholars of XYNU. The authors acknowledge the master students Qianqian Wei and Xiaoyue Ding for their assistance in the evaluation of biocompatibility and antibacterial properties. In addition, Lei Nie acknowledges the discussion, argument, explanation and support from YY. The authors acknowledge the help from Prof. Qiuju Zhou, Miss Zihe Jin, Dr. Zongwen Zhang, and Dr. Dongli Xu, in the Analysis & Testing Center of XYNU.

References

[1] Dave U, Somanader E, Baharlouei P, Pham L, Rahman MA. Applications of Chitin in Medical, Environmental, and Agricultural Industries. 2021;9(11):1173.

[2] Mohan K, Ganesan AR, Ezhilarasi PN, Kondamareddy KK, Rajan DK, Sathishkumar P, et al. Green and eco-friendly approaches for the extraction of chitin and chitosan: A review. Carbohydrate Polymers. 2022;287:119349.

[3] Croisier F, Jérôme C. Chitosan-based biomaterials for tissue engineering. European Polymer Journal. 2013;49(4):780-92.

[4] Fatimi A, Okoro OV, Podstawczyk D, Siminska-Stanny J, Shavandi A. Natural Hydrogel-Based Bio-Inks for 3D Bioprinting in Tissue Engineering: A Review. 2022;8(3):179.

[5] Luan F, Wei L, Zhang J, Tan W, Chen Y, Dong F, et al. Preparation and Characterization of Quaternized Chitosan Derivatives and Assessment of Their Antioxidant Activity. Molecules. 2018;23(3).

[6] Chen M, Feng X, Liu J, Liu Y, Bai Y, Wang Z. Investigation on preparation of carboxymethyl chitosan modified sodium ferric silicate and its adsorption properties. 2021;27(4):841-54.

[7] Wang W, Meng Q, Li Q, Liu J, Zhou M, Jin Z, et al. Chitosan Derivatives and Their Application in Biomedicine. 2020;21(2):487.

[8] Pires NR, Cunha PLR, Maciel JS, Angelim AL, Melo VMM, de Paula RCM, et al. Sulfated chitosan as tear substitute with no antimicrobial activity. Carbohydrate Polymers. 2013;91(1):92-9.
[9] Jesús M-ST, Hernán H-MC, Rubén R-NJ. An overview of the chemical modifications of chitosan and their advantages. 2018;6(4):131-42.
[10] Ahmadi F, Oveisi Z, Samani SM, Amoozgar Z. Chitosan based hydrogels: characteristics and pharmaceutical applications. Research in pharmaceutical sciences. 2015;10(1):1-16.
[11] Pinto RV, Gomes PS, Fernandes MH, Costa MEV, Almeida MM. Glutaraldehyde-crosslinking chitosan scaffolds reinforced with calcium phosphate spray-dried granules for bone tissue applications. Materials Science and Engineering: C. 2020;109:110557.
[12] Jalalvandi E, Shavandi A. In situ-forming and pH-responsive hydrogel based on chitosan for vaginal delivery of therapeutic agents. Journal of Materials Science: Materials in Medicine. 2018;29(10):158.
[13] Shavandi A, Bekhit AE-DA, Sun Z, Ali MA. Injectable gel from squid pen chitosan for bone tissue engineering applications. Journal of Sol-Gel Science and Technology. 2016;77(3):675-87.
[14] Nie L, Deng Y, Li P, Hou R, Shavandi A, Yang S. Hydroxyethyl Chitosan-Reinforced Polyvinyl Alcohol/Biphasic Calcium Phosphate Hydrogels for Bone Regeneration. ACS Omega. 2020;5(19):10948-57.
[15] Nie L, Chen D, Zhong S, Shi Q, Sun Y, Politis C, et al. Injectable cell-laden poly(N-isopropylacrylamide)/chitosan hydrogel reinforced via graphene oxide and incorporated with dual-growth factors. Materials Letters. 2020;280:128572.
[16] Nie L, Li J, Lu G, Wei X, Deng Y, Liu S, et al. Temperature Responsive Hydrogel for Cells Encapsulation Based on Graphene Oxide Reinforced poly (N-isopropylacrylamide)/Hydroxyethyl-Chitosan. Mater Today Commun. 2022:103697.
[17] Jafari H, Delporte C, Bernaerts KV, Alimoradi H, Nie L, Podstawczyk D, et al. Synergistic complexation of phenol functionalized polymer induced in situ microfiber formation for 3D printing of marine-based hydrogels. Green Chemistry. 2022;24(6):2409-22.
[18] Jafari H, Ghaffari-bohlouli P, Podstawczyk D, Nie L, Shavandi A. Tannic acid post-treatment of enzymatically crosslinked chitosan-alginate hydrogels for biomedical applications. Carbohydrate Polymers. 2022:119844.
[19] Liu S, Zhao Y, Wei H, Nie L, Ding P, Sun H, et al. Injectable hydrogels based on silk fibroin peptide grafted hydroxypropyl chitosan and oxidized microcrystalline cellulose for scarless wound healing. Colloids and Surfaces A: Physicochemical and Engineering Aspects. 2022:129062.
[20] Deng Y, Shavandi A, Okoro OV, Nie L. Alginate modification via click chemistry for biomedical applications. Carbohydrate Polymers. 2021;270:118360.
[21] Guaresti O, Basasoro S, González K, Eceiza A, Gabilondo N. In situ cross–linked chitosan hydrogels via Michael addition reaction based on water–soluble thiol–maleimide precursors. European Polymer Journal. 2019;119:376-84.
[22] Teng D-y, Wu Z-m, Zhang X-g, Wang Y-x, Zheng C, Wang Z, et al. Synthesis and characterization of in situ cross-linked hydrogel based on self-assembly of thiol-modified chitosan with PEG diacrylate using Michael type addition. Polymer. 2010;51(3):639-46.
[23] Van Hoorick J, Tytgat L, Dobos A, Ottevaere H, Van Erps J, Thienpont H, et al. (Photo-)crosslinkable gelatin derivatives for biofabrication applications. Acta biomaterialia. 2019;97:46-73.
[24] Wang Y, Zhang S, Wang JJCCL. Photo-crosslinkable hydrogel and its biological applications. 2021;32(5):1603-14.
[25] Zeng Z, Mo X-m, He C, Morsi Y, El-Hamshary H, El-Newehy M. An in situ forming tissue adhesive based on poly (ethylene glycol)-dimethacrylate and thiolated chitosan through the Michael reaction. Journal of Materials Chemistry B. 2016;4(33):5585-92.

[26] Rahali K, Ben Messaoud G, Kahn CJF, Sanchez-Gonzalez L, Kaci M, Cleymand F, et al. Synthesis and Characterization of Nanofunctionalized Gelatin Methacrylate Hydrogels. Int J Mol Sci. 2017;18(12).
[27] Nie L, Wang C, Hou R, Li X, Sun M, Suo J, et al. Preparation and characterization of dithiol-modified graphene oxide nanosheets reinforced alginate nanocomposite as bone scaffold. Sn Applied Sciences. 2019;1(6):1-16.
[28] Akhramez S, Fatimi A, Okoro OV, Hajiabbas M, Boussetta A, Moubarik A, et al. The Circular Economy Paradigm: Modification of Bagasse-Derived Lignin as a Precursor to Sustainable Hydrogel Production. 2022;14(14):8791.
[29] Nie L, Chang P, Liang S, Hu K, Hua D, Liu S, et al. Polyphenol rich green tea waste hydrogel for removal of copper and chromium ions from aqueous solution. Cleaner Engineering and Technology. 2021;4:100167.
[30] Zhou L, Tan G, Tan Y, Wang H, Liao J, Ning C. Biomimetic mineralization of anionic gelatin hydrogels: Effect of degree of methacrylation. RSC Advances. 2014;4(42):21997-2008.
[31] Zhao W, Kong M, Feng C, Cheng X, Liu Y, Chen X. Investigation of gelling behavior of thiolated chitosan in alkaline condition and its application in stent coating. Carbohydrate Polymers. 2016;136:307-15.
[32] MERCK. IR Spectrum Table & Chart. Darmstadt: Merck KGaA; 2022.
[33] Nie L, Zou P, Feng S, Suo J. Temperature-sensitive star-shaped block copolymers hydrogels for an injection application: Phase transition behavior and biocompatibility. Journal of Materials Science: Materials in Medicine. 2013;24(3):689-700.
[34] Zou P, Suo J, Nie L, Feng S. Temperature-sensitive biodegradable mixed star-shaped block copolymers hydrogels for an injection application. Polymer. 2012;53(6):1245-57.
[35] Kumari S, Malvi B, Ganai AK, Pillai VK, Sen Gupta S. Functionalization of SBA-15 mesoporous materials using “thiol–ene click” Michael addition reaction. The Journal of Physical Chemistry C. 2011;115(36):17774-81.
[36] Jang J, Seol Y-J, Kim HJ, Kundu J, Kim SW, Cho D-W. Effects of alginate hydrogel cross-linking density on mechanical and biological behaviors for tissue engineering. Journal of the Mechanical Behavior of Biomedical Materials. 2014;37:69-77.
[37] Collins MN, Birkinshaw C. Morphology of crosslinked hyaluronic acid porous hydrogels. Journal of Applied Polymer Science. 2011;120(2):1040-9.
[38] Luo Q, Han Q, Wang Y, Zhang H, Fei Z, Wang Y. The thiolated chitosan: Synthesis, gelling and antibacterial capability. International journal of biological macromolecules. 2019;139:521-30.
[39] Huang L, Zhu Z, Wu D, Gan W, Zhu S, Li W, et al. Antibacterial poly (ethylene glycol) diacrylate/chitosan hydrogels enhance mechanical adhesiveness and promote skin regeneration. Carbohydrate polymers. 2019;225:115110.
[40] Zhang H, Qadeer A, Chen W. In Situ Gelable Interpenetrating Double Network Hydrogel Formulated from Binary Components: Thiolated Chitosan and Oxidized Dextran. Biomacromolecules. 2011;12(5):1428-37.